

# THELI – Convenient reduction of optical, near- and mid-infrared imaging data

M. Schirmer<sup>1,2,3</sup>

<sup>1</sup>*Gemini Observatory, Casilla 603, La Serena, Chile;*  
mschirme@gemini.edu

<sup>2</sup>*Isaac Newton Group of Telescopes, Santa Cruz de La Palma, Spain*

<sup>3</sup>*Argelander-Institut für Astronomie, Universität Bonn, Germany*

## ABSTRACT

The last 15 years have seen a surge of new multi-chip optical and near-IR imagers. While some of them are accompanied by specific reduction pipelines, user-friendly and generic reduction tools are uncommon. In this paper I introduce THELI, an easy-to-use graphical interface driving an end-to-end pipeline for the reduction of any optical, near-IR and mid-IR imaging data. The advantages of THELI when compared to other approaches are highlighted. Combining a multitude of processing algorithms and third party software, THELI provides researchers with a single, homogeneous tool. A short learning curve ensures quick success for new and more experienced observers alike. All tasks are largely automated, while at the same time a high level of flexibility and alternative reduction schemes ensure that widely different scientific requirements can be met. Over 90 optical and infrared instruments at observatories world-wide are pre-configured, while more can be added by the user. The online Appendices contain three walk-through examples using public data (optical, near-IR and mid-IR). Additional extensive online documentation is available for training and troubleshooting.

*Subject headings:* Techniques: image processing

## 1. Introduction

The systematic introduction of CCDs revolutionized the field of observational astronomy at the beginning of the 1980s (see e.g. Crane et al. 1981; Goad & Ball 1981; Gunn & Westphal 1981; McLean et al. 1981; Mortara & Fowler 1981). It was paralleled by the development of large software packages to process these new kinds of data, such as IRAF (Butcher & Stevens 1981; Valdes 1984), ESO-MIDAS (Banse et al. 1983), and STARLINK (Pavelin & Walter 1980). These programs have become deeply tied to observational astronomy. They form an integral part of the observing and data acquisition software at many observatories, and numerous reduction packages have been built on them.

At the end of the 1990s the limited field of view of a single CCD was overcome by mosaic cameras, such as (in the optical) WFI at the Anglo-Australian Observatory (AAO), WFI at the 2.2m MPG/ESO tele-

scope (Baade et al. 1999), CFH12K at the Canada-Hawaii-France Telescope (CFHT, Cuillandre et al. 2000), and SuprimeCam at Subaru (Miyazaki et al. 2002), and in the near-IR CIRSI at the William Herschel Telescope (WHT, Beckett et al. 1997). In the following, these and other instrument / telescope combinations will be abbreviated as in e.g. WFI@AAO. Deep and wide surveys have become possible since then, drastically increasing the volume of data produced per night. While the new instruments have been used frequently from the start, the volumes and much increased complexity of the data have proved a challenge for the first few years as corresponding software support lagged behind. In particular astrometric and photometric solutions have become non-trivial and tiresome, now that dithered images from detector mosaics with distortion patterns have to be combined. This has triggered the development of many astrometric pipelines outside the IRAF or MIDAS context,

such as WIFIX<sup>1</sup>, the LDAC pipeline<sup>2</sup>, and Scamp (Bertin 2006), to name just a few.

New survey telescopes such as the VST, VISTA, and the future LSST are pushing the boundaries further, combining extreme optics with detector mosaics of up to a hundred CCDs or more (e.g. DECam@CTIO, Flaugher et al. (2012); GPC1@Pan-Starrs, Onaka et al. (2008); HyperSuprimeCam@Subaru, Miyazaki et al. (2012); ODI@WIYN, Jacoby et al. (2002); OmegaCam@VST, Kuijken et al. (2002); VIRCAM@-VISTA, Hummel et al. (2010)). While some of these cameras are mostly used for public surveys, others are facility instruments available for private investigators (PIs). The associated data reduction pipelines are not necessarily publicly available (e.g. VISTA) or portable to the PI's computer, as they may be tied to large commercial data base applications.

Data processing is made even more challenging by the multitude of optical and near-IR data we combine for our research. It is common that exposures from several telescopes and cameras are pooled for one project, providing sufficient sample sizes and/or a multi-wavelength perspective. Frequently, researchers have to switch to new and unfamiliar software to ensure consistent data quality, a time-consuming and demanding task. Custom-made reduction scripts and methods are often no longer interchangeable between instruments.

In 2000, Thomas Erben and I faced these problems for our 20 square degree weak lensing survey (Schirmer et al. 2003), and decided to develop an instrument-independent pipeline that could process data from any future, optical multi-chip camera. We exploited existing, stand-alone software solutions (mostly Astromatic<sup>3</sup> and LDAC), and merged them with custom-made modules to ensure a fast and smooth data flow. This THELI pipeline core is operated by a number of command-line scripts, and has been developed on data from WFI@2.2m MPG/ESO and MegaCam@CFHT. Its main purpose is the reduction of large survey data sets, such as the CFHTLenS (Erben et al. 2013), utilizing Linux cluster architectures. The pipeline, presented in Erben et al. (2005) (hereafter E05), has been extensively tested (e.g. Hildebrandt et al. 2006; Erben et al. 2013).

The command-line approach for mass production

competed with the goal for an instrument-independent pipeline to be used by a PI for his or her individual projects. Hard-coded parameters and manual editing of configuration files were just some of the obstacles. Another problem is that the command-line scripts have been optimised for the reduction of blank fields, and do not work (well) for crowded fields or significantly extended sources. To overcome these issues I started developing a THELI graphical user interface (GUI). It includes many new tasks such as alternative astrometric routines and more adaptive sky subtraction methods. In addition to full near- and mid-IR support it also handles all administrative tasks for the user. Thus, a highly flexible and convenient tool able to process essentially all kinds of imaging data now exists. It facilitates a broad range of scientific studies, ranging e.g. from the optical distortion modeling of the LORRI camera on-board the *New Horizons* mission (McMichael & Bentley 2012) or the *Deep Impact* campaign (Meech et al. 2005), via the expansion history of planetary nebulae (Santander-García et al. 2008) to studies of galaxy clusters (Lieder et al. 2012). THELI's command-line version has been used for several large survey projects, such as a systematic lensing study of 51 of the most X-ray luminous galaxy clusters known (von der Linden et al. 2012), and the CFHT Lensing Survey (CFHTLenS, comprising 154 square degrees; Heymans et al. 2012).

This paper contains a description of the THELI GUI's (version 2.8.1) most important features. An additional comprehensive user manual and technical reference is available online<sup>4</sup>. For the remainder of this paper, 'THELI' refers to the GUI. Section 2 contains a short overview of the working principle, and discusses software pre-requisites for installation. Section 3 covers the preparation of the data, non-linearity and cross-talk corrections. In Section 4 the various options available for background modeling are explained. This is followed by a short summary about weighting and bad pixel mapping in Sect. 5, with astrometric and photometric calibration in Sect. 6. Sky modeling is addressed in Sect. 7, and the various options available for final image coaddition in Sect. 8. A short summary and outlook is presented in Sect. 9. Appendices A through C (online material) contain three step-by-step reduction examples, based on public optical, near-IR, and mid-IR images. A list of currently supported instruments is included at the end.

<sup>1</sup>M. Radovich, <http://www.na.astro.it/~radovich/wifix.htm>

<sup>2</sup>E. Deul, <ftp://ftp.strw.leidenuniv.nl/pub/ldac/software/>

<sup>3</sup><http://www.astromatic.net>

<sup>4</sup><http://www.astro.uni-bonn.de/~theli/gui>

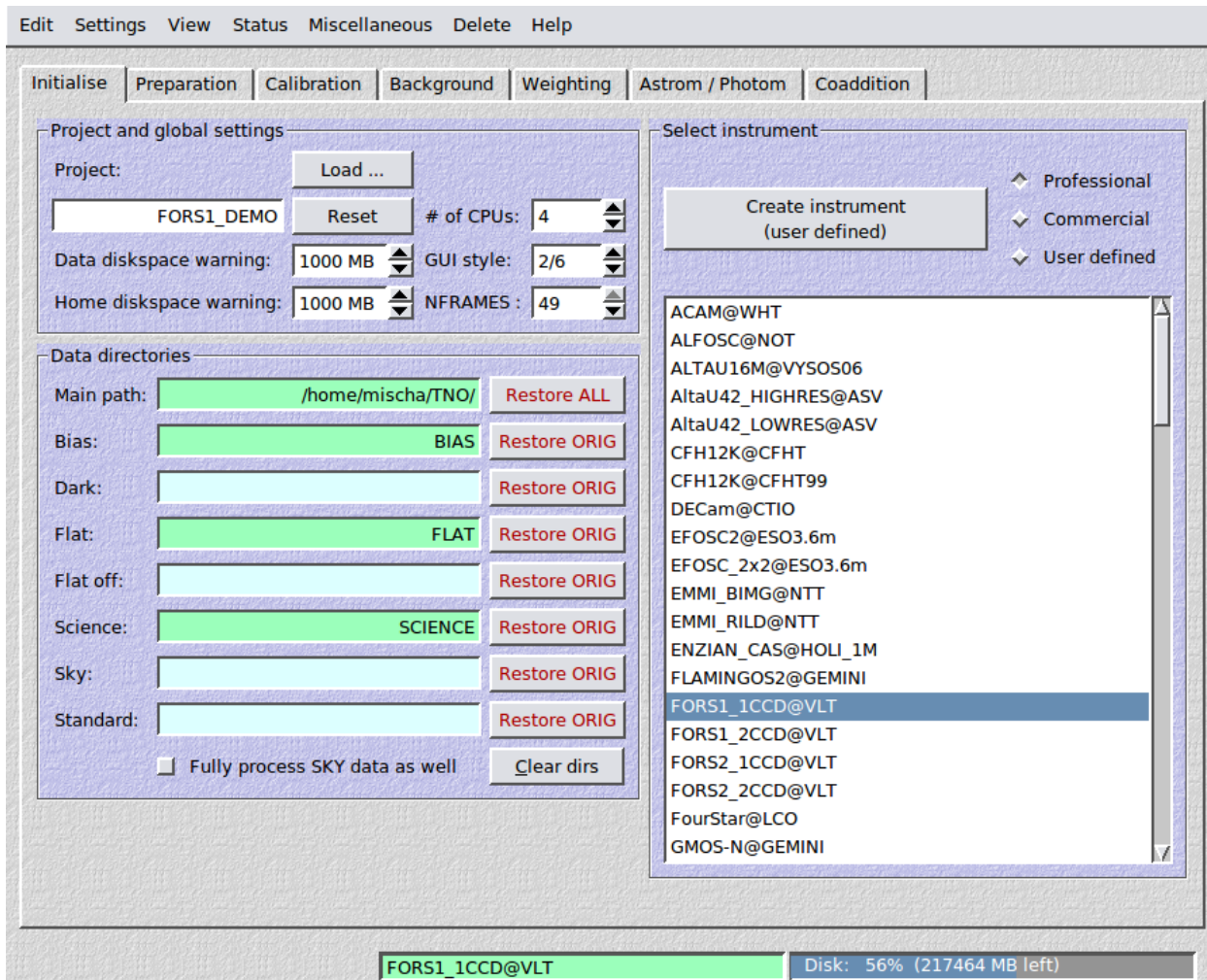


Fig. 1.— Initial setup of a new data reduction project in THELI.

## 2. Structure and operation of THELI

Most data processing algorithms in THELI are not new inventions, but have been used before. The big advantage of THELI is that a multitude of these procedures has been combined and made accessible in a single, homogeneous tool. Figure 1 shows the *Initialise* section of THELI’s user interface, where global information is provided, such as the current project title, how many CPUs to use, where the data can be found, and the instrument they were taken with. Thereafter, the user steps through six sections to arrive at a coadded image. The main aspects of these sections are discussed in this paper, with concrete examples given in the appendices.

### 2.1. Software pre-requisites and implementation

Most software modules developed for THELI, as well as third party programs such as the *Astromatic* tools, are written in C/C++. They are compiled with standard tools such as *gcc* and *make*, and do not require exotic libraries. A few other modules are based on the *python* language. The user interface itself is based on the C/C++ *Qt* library, which is also the heart of many Desktop environments such as KDE. All these pre-requisites are fundamental parts of modern Linux systems and available in pre-compiled form in their respective repositories. As such, THELI can be compiled on essentially all Linux platforms and has sufficient backwards compatibility.

The only current shortcoming is that THELI does not compile under MacOS<sup>5</sup>. This can be overcome by installing a Linux guest operating system in a virtual machine, at the cost of performance. THELI is currently based on Qt3, which is being phased out in future Linux releases, but can always be compiled from source<sup>6</sup>. In the near future, THELI will be ported to the recently released Qt5 library, and offer full support for MacOS.

### 3. Correcting headers and detector features

#### 3.1. Homogenizing FITS headers

The first step in THELI is to bring all FITS headers from different instruments to a common format, taking into account possible header changes made over time. This is essential for an instrument-independent pipeline to work, as not all FITS headers adhere to the FITS standard<sup>7</sup>. For example, conflicting keywords such as CD*i* and PC*i* may appear simultaneously, or the instrument’s orientation on sky is unknown. Likewise, the WCS information may be inaccurate or have to be reconstructed from nonstandard keywords. Invalid key values such as negative airmass have to be corrected as well. More intricate problems such as incorrect filter names can in general not be detected automatically. Thus it is the user’s responsibility to validate the integrity of the raw data.

Consequently, THELI modifies the original FITS header, retaining and translating only keywords essential for the data reduction. Apart from mandatory keywords, the new header comprises a complete set of WCS keys, date and time, plus a few others such as airmass, filter and exposure time. Additional keywords to be retained can be defined by the user. Multi-extension FITS files are split into individual chips for parallelisation purposes at this point of the processing.

#### 3.2. Cross-talk

Different forms of cross-talk (Fig. 2) may appear in detectors with multiple readout channels. *Intra-chip normal cross-talk* causes ghost images of a bright source in the other channels. *Row cross-talk* enhances the values of the rows (or columns) containing a bright source, and the same feature is projected into the other

readouts (for an example see Freyhammer et al. 2001). These effects are fixed by subtracting a rescaled image (or scaled average row values) of the offending channel from the other channels. Both forms of cross-talk may appear simultaneously.

*Inter-chip cross-talk* can occur in multi-chip cameras, e.g. WFC@INT, DECam@CTIO and OmegaCam@VST, creating ghost image of one chip in another chip. It can be corrected by image subtraction, a mode that is currently being implemented in THELI.

Some HAWAII 2048×2048 arrays show *edge cross-talk*, recognized by positive and negative amplitudes within a ring-shaped ghost. Albert et al. (2008) show that this can be solved for on a hardware level. THELI can in principle also correct for this effect. However, results have not been satisfactory for the cameras tested (HAWK-I@VLT, VIRCAM@VISTA, Flamingos2@Gemini), as the amplitudes of the ghosts vary between channels.

In general, cross-talk amplitudes may be positive or negative, i.e. the ghost images can be bright or dark. Their amplitudes are typically a factor 10<sup>4</sup> smaller than the sources, but may become as large as 0.025, e.g. for NICS@TNG. Corrections work best if the offending sources are not saturated. Cross-talk severely compromises the data from crowded fields and deep observations, as the ghosts are fixed with respect to the sources and thus do not appear as outliers in a set of dithered images. By choosing different sky position angles, however, cross-talk can be statistically identified and removed.

#### 3.3. Non-linearity

THELI’s non-linearity correction is represented by a third-order polynomial,

$$x_{\text{lin}} = \sum_{i=0}^3 a_i x_0^i, \quad (1)$$

where  $x_0$  are the pixel values in the uncorrected exposure. The coefficients ( $a_i$ ) are stored in a separate configuration file. Currently, only a few instruments (such as WFC@INT) are pre-configured for non-linearity correction. Coefficients for other instruments can be added by the user.

After these preparatory steps, the user creates a master bias and a master flat, and applies them to the data. This is a straightforward process and described in the example reductions in the appendices.

<sup>5</sup>The command-line version, however, using the pipeline core only, does compile under MacOS.

<sup>6</sup><http://download.qt-project.org/archive/qt/3/>

<sup>7</sup>[http://fits.gsfc.nasa.gov/fits\\_standard.html](http://fits.gsfc.nasa.gov/fits_standard.html)

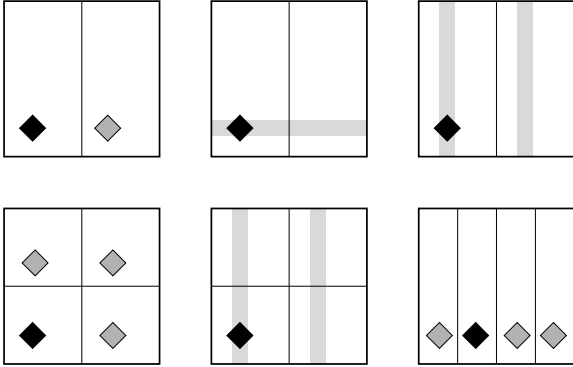


Fig. 2.— Various cross-talk effects. The offending source and its ghosts from normal cross-talk are shown as black and gray diamonds, respectively. Shaded gray lines represent row cross-talk. The thin lines mark the readout sections. Both normal and row cross-talk can appear simultaneously.

#### 4. Background modeling and zero-point variations

THELI distinguishes between *background modeling* and *sky subtraction*. A background model is a median combination of several successive and dithered exposures, correcting for residual variations after flat-fielding. Depending on the cause of the variations, the images must be divided (‘superflatted’) by the model, or the model is subtracted. The latter is typically the case for near-IR observations and removes most of the sky signal. Sect. 4.1 and 4.1.1 show different ways of creating a background model. *Sky subtraction*, on the other hand, is based on single images and eliminates any remaining individual gradients or pedestals (see Sect. 7).

Background variations may vary over time. Possible causes include both additive and multiplicative effects, such as

- improper illumination of the dome/flat screen,
- scattered light in twilight flats,
- moonlight,
- airglow (particularly in the near-IR),
- sky concentration (reflection between CCD and corrector lenses or filters),
- fringing.

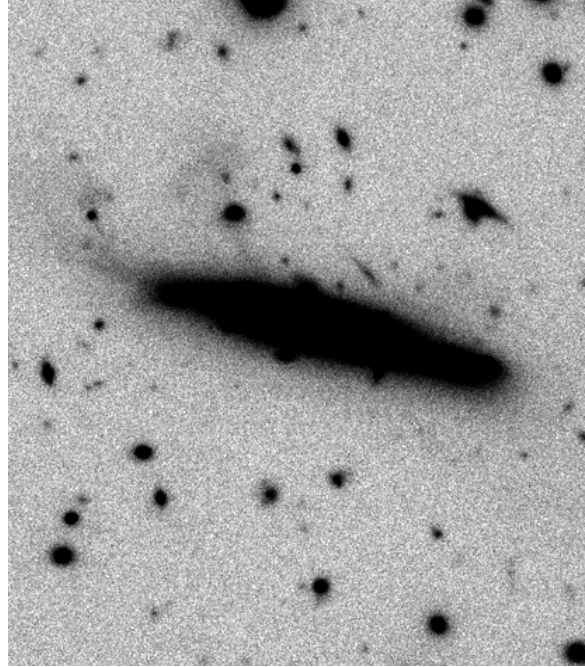


Fig. 3.— Deep HAWK-I *J*-band image of an anonymous field galaxy. A faint tidal plume and other debris from minor mergers are clearly visible, demonstrating the quality of THELI’s near-IR background modeling.

Spatial zero-point variations occur when additive and multiplicative components are mixed in a flat field. They result either from external scattering (e.g. unfavorable dome orientation during twilight), or internal reflections in the instrument. The amplitudes of these variations can reach up to 10%. A direct comparison of stellar magnitudes in dithered data is required. A comparison with known reference sources in the field can also be performed to solve this problem (Manfroid et al. 2001; Koch et al. 2004). The latter approach is available in THELI (Sect. 6.1), yielding single zero-point adjustments for individual chips but not yet a full 2D correction. For instruments that are mostly used for survey work, the corresponding 2D corrections are usually included in a dedicated pipeline (e.g. VIRCAM@VISTA), or directly applied to pre-processed archival data (e.g. MegaCam@CFHT, using the ELIXIR pipeline; Magnier & Cuillandre 2004).

##### 4.1. Static and dynamic background models

A *static background model* is a single median image created from a series of exposures. It can be ap-

plied to all images from which it was created, and is rescaled to correct for slow, global variations. A good example is a background model created from a 10 – 30 minute long sequence of short near-IR exposures. Atmospheric airglow changes little during this time, and thus a single static model is sufficient to subtract the sky. Another case would be a classic optical superflat computed from data taken on a clear night.

A *dynamic background model* is needed if sky conditions are unstable during a series of exposures. This is generally the case for any near-IR sequence extending over more than 10 – 30 minutes, as the airglow changes the sky brightness on time scales of minutes with spatial fluctuations on scales of arcminutes. Optical *i*- or *z*-band data may also require dynamic correction. THELI creates the background model for the *k*-th exposure from the *m* closest exposures in time. The latter may or may not bracket the *k*-th exposure symmetrically.

Common to both approaches is that all objects are masked prior to the creation of the model, and the highest pixel in the stack is rejected. These settings can be adjusted arbitrarily. THELI also supports two-pass background subtraction, which may be required in the near-IR for extended objects or very deep observations (see App. B for an example processing flow). The quality of THELI’s background models is illustrated in Fig. 3, revealing two extended tidal debris features of low surface brightness around a random field galaxy (see also Martínez-Delgado et al. 2010).

An exposure sequence containing one or more longer interruptions is not adequately represented by a single background model. If the interruptions exceed a user-specified amount of time, separate background models are automatically calculated for each group of images and applied accordingly.

#### 4.1.1. Separate sky observations

The variable near-IR background requires larger dither patterns in the presence of extended objects to be able to estimate the sky at the object’s position. A nearby blank field has to be observed in a periodic manner if the target comprises about half the detector’s field-of-view or more. This may also become necessary for optical observations if an accurate correction is required. Exposures of a blank area should be kept in a separate SKY directory where they are found and processed by THELI.

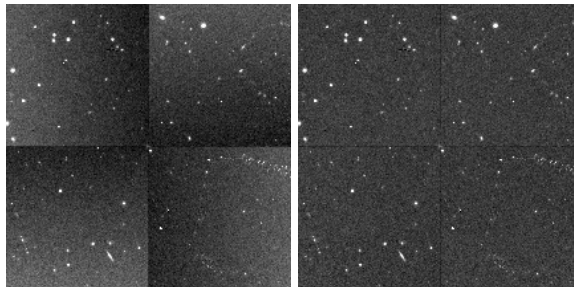


Fig. 4.— Left: Single MOIRCS@SUBARU *J*-band exposure after background modeling, showing a reset anomaly in the four quadrants (data from Uchimoto et al. 2012). Right: After correction.

## 4.2. Removing linear gradients

Some HAWAII arrays show residual linear gradients after background modeling, leading to discontinuities between readout quadrants. This *detector reset anomaly* may depend on exposure time, sky brightness, the time passed between exposures, detector temperature, etc. It is corrected by subtracting an average row or column calculated from the affected area. This *collapse correction* also supports HAWAII-2 arrays with 4 quadrants and alternating 90 degree orientation (see Fig. 4).

## 4.3. Mid-IR observations

Ground-based mid-IR observations require special observing techniques as the background signal is very high ( $-5$  to  $-7$  mag/arcsec<sup>2</sup>). To remove the rapidly varying sky, the secondary mirror is tilted (*chopped*) every few seconds, projecting an empty sky area in the immediate vicinity of the target onto the detector. The second image is then subtracted from the first one. But the thermal signal from the telescope does not cancel out entirely, since the detector sees the telescope from slightly different angles at the two chopper positions. The telescope is therefore offset slightly (a process known as *nodding*), and another series of chopped images taken at the new position. A new difference image is calculated from the chopped images at the second nod position. Finally, by subtracting it from the first difference image, the residual thermal signal is removed. If the order of science and sky observations are reversed at the 2nd nod position, the difference images have to be added (see Fig. 5). As the telescope’s temperature changes only slowly, the nodding is usually done once or twice per minute.

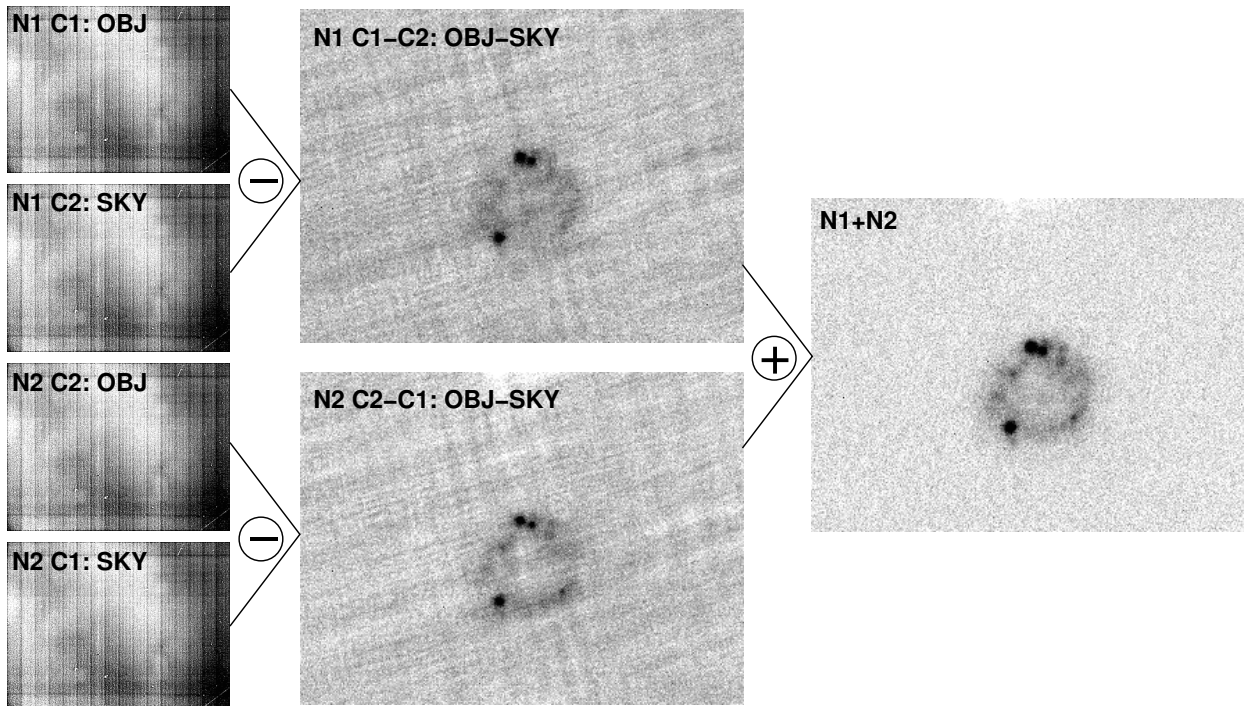


Fig. 5.— Chop-nod observations of the starburst ring in NGC 7552, observed with T-ReCS@GEMINI in the  $[\text{Si II}]$   $8.8\mu\text{m}$  bandpass. N1/2 and C1/2 refer to the nod and chop positions. With T-ReCS, the science target is observed at C2 instead of C1 when at nod position 2. The residual telescopic thermal background visible in the difference images (middle column) is therefore inverted. The sum of the difference images hence yields the corrected image (right).

Data formats and the amount of information stored in the raw data vary greatly between mid-IR instruments. T-ReCS@GEMINI, for example, averages the two-dimensional individual exposures obtained at a given chop/nod position and sorts them into a 4-dimensional hyper-cube, where the two extra dimensions specify (1) the telescope’s nod position, and (2) whether the chopper observed the sky or the target. Sky exposures with T-ReCS are unguided and generally discarded after processing due to inferior quality. A typical chop-nod cycle lasts several minutes, and is stored as one hyper-cube. An arbitrary number of such hyper-cubes may be contained in separate FITS extensions. THELI performs the chop-nod sky subtraction during initial data preparation. It writes out either a single 2D FITS image, representing the fully stacked hyper-cube, or one image for every chop-nod cycle.

The other currently supported mid-IR camera is VISIR@VLT. Currently a generic chop-nod module is available for thermal background removal. This will be replaced by individually optimized routines (such

as for T-ReCS) once more mid-IR cameras are implemented in THELI. A VISIR image processed with THELI is shown in Fig. 6.

## 5. Weighting and defect detection

The general weighting process has been described in detail in E05. To summarize, a weight map is created based on the normalized flat. This *global weight* is then modified individually to mask cosmics, hot pixels or satellites present in the images.

Many CCDs suffer from bad columns, some of which cannot be corrected using dark exposures. THELI is able to identify such defects (even weak ones) in a well exposed flat field. The variations in a flat field due to uneven illumination are often larger than those caused by bad columns. These effects must therefore first be corrected for, which is done by dividing the flat field by itself after convolution with a 30 pixel wide Gaussian. The mean value of an individual column is then compared to the overall mean of the image. The column will be masked if it deviates by

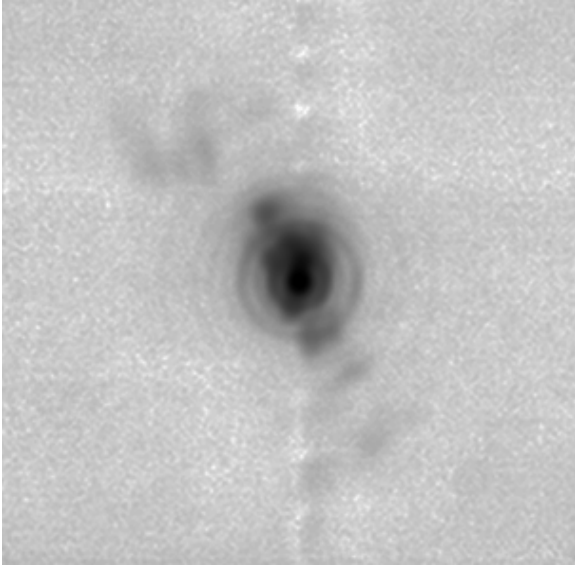


Fig. 6.— The center of the Seyfert 2 galaxy NGC 1068, as seen in [NeII]  $12.8\mu\text{m}$  with VISIR@VLT. Note the circularly symmetric diffraction rings.

more than a user-defined threshold (default: 2%).

## 6. Photometry and astrometry

### 6.1. Direct photometric calibration

*Direct* photometric calibration means that the zero-point of an individual exposure is obtained from stars of known magnitude within the same field. Currently, SDSS-DR9 (Ahn et al. 2012) and 2MASS (Skrutskie et al. 2006) catalogs are available in THELI for this purpose. A (configurable) maximum uncertainty of 0.05 mag is allowed for the reference magnitudes. Future deeper/wider surveys will be implemented as they become publicly available.

This method has three advantages compared to the classic *indirect* calibration. First, the data can be taken in arbitrary photometric conditions. Second, multi-chip cameras can be corrected for residual zero-point differences between chips (see e.g. Schirmer et al. 2011). Third, no observing time has to be reserved for standard stars at different airmass. On the downside, possible color terms remain undetermined.

### 6.2. Indirect photometric calibration

In E05 we describe photometric calibration using standard stars and a three parameter fit (zero-point,

color term, extinction). Only the bright *UBVRI* standards by Landolt (1992) and Stetson (2000) were implemented at the time. Today THELI provides the SDSS stripe 82 photometric calibration catalog (Ivezić et al. 2007) in addition, covering  $20:30:00 < \text{RA} < 04:00:00$ , and  $-01:16:00 < \text{DEC} < 01:16:00$ . Originally this catalog contains 1.01 million point sources, but only objects with photometric errors  $< 0.05$  mag in all bands are kept. Very faint sources in the *gri* filters, which could lead to a systematic bias of 0.02 mag in the zero-point, have also been removed. 340 000 sources remain, all of which have *ugriz* magnitudes in the SDSS 2.5m system as well as *u'g'r'i'z'* in the USNO 1.0m system (Smith et al. 2007). The catalog has to be downloaded separately from the THELI webpage.

For near-IR data,  $JHK_s$  magnitudes from Leggett et al. (2006) (UKIRT MKO), Hunt et al. (1998) and Persson et al. (1998) are available, as well as the 2MASS calibration fields by Nikolaev et al. (2000). A combined  $YJHK_sLM$  catalog from UKIRT/JAC has also been added, together with  $L'M'$  data from Leggett et al. (2003).

### 6.3. Astrometry

Astronomical instruments cover very small to very large fields of view, hence absolute astrometric calibrations rely on suitably chosen reference catalogs. Extreme cases are e.g. near-IR data of a small field with low source density, or wide-field images of the crowded galactic plane. Successful matching of source and reference catalogs requires sufficient mutual overlap. A variety of adjustments are available if matching with default values fails:

- Depth of the reference catalog (to avoid computational limits for crowded fields)
- Depth of the SExtractor (Bertin & Arnouts 1996) source catalog
- Deblending of composite sources (e.g. richly structured galaxies)
- Filters to reject spurious sources
- Various reference catalogs (e.g. for greater depth or better wavelength match)
- Different matching algorithms

Currently implemented catalogs are SDSS-DR9, PPMXL, USNO-B1, 2MASS, UCAC-4, GSC-2.3 and TYCHO (Ahn et al. 2012; Roeser et al. 2010; Monet et al. 2003; Cutri et al. 2003; Zacharias et al. 2012; Lasker et al. 2008; Perryman & ESA 1997, respectively). TYCHO can be used for images taken with wide angle photo lenses covering hundreds of square degrees. For all-sky camera data, a locally stored, filtered version of GSC-2.3 with an upper magnitude limit of 10 is available.

Sometimes these catalogs are insufficient, e.g. if the target is a bright and richly structured nearby galaxy. The reference catalog might then be empty because the photographic plate was saturated, or the source deblending insufficient. In this case, secondary reference catalogs can be created with THELI from images with valid WCS headers taken with another telescope (see e.g. Sect. 6.3.5).

The astrometric solution is stored in separate FITS headers, which are read by SWarp (Bertin 2010) during image coaddition. The individual images remain uncorrected, unless the *Update header* function is used, inserting the first order solution (CRPIX1/2, CRVAL1/2, and CDi,j) into the headers. This is optional and can be undone anytime. If fully distortion-corrected individual images are needed the resampled data (Sect. 8.1.1) can be utilized.

### 6.3.1. Scamp

The most commonly used astrometric tool in THELI is Scamp (Bertin 2006), developed in particular for multi-chip cameras. Previously stored information about the detectors' relative orientation (the *focal plane*, hereafter FP) can be used. To this end the FP has been measured for all pre-configured multi-chip cameras in THELI (Tables 4 and 5, App. D) based on dense stellar fields. FP models may need updates from time to time, e.g. if an instrument has undergone mechanical or optical maintenance. In cases where the detectors are not located in the same physical plane (e.g. VIMOS@VLT, SPARTAN@SOAR), differential flexure between the optical arms may require the FP model to be updated for each data set. This functionality is readily available in THELI.

The internal accuracy of the resulting astrometric solution with Scamp is on the order of 0.06 – 0.12 pixels for optical wide-field imagers (see e.g. Erben et al. 2013). For low density fields observed in the near-IR it may be reduced to 0.1 – 0.3 pixels. Once the astromet-

ric solution is obtained, Scamp also determines relative photometric zero-points for the exposures.

Scamp matches the object catalogs to the astrometric reference catalog as follows. In the first step, the pixel scale and relative position angle are determined for both catalogs by “*cross-correlating the 2D histograms of source pair coordinates in the  $\log(\text{separation})$  vs.  $\text{position-angle}$  space*” (Bertin 2006; Kaiser et al. 1999). The offset in RA and DEC is found by correlating the 2D positional histograms. This approach works well as long as the positional uncertainty is not too large, i.e. the offset between nominal and true coordinates is not larger than about half the field of view. However, this condition is not always met, which can make the astrometric solution difficult (in particular if the position angle and a possible flip are still undetermined, e.g. for commissioning data).

### 6.3.2. Astrometry.net

A complementary solution to Scamp is a local implementation of the *astrometry.net* algorithm (Lang et al. 2010). Matching is based on quadrilaterals in the reference and the object catalogs. *astrometry.net* can create its own source catalogs, but in THELI it will use the same SExtractor catalogs as created for Scamp. In this way the user has more control over source densities and spurious detections. THELI does not use the *astrometry.net* all-sky online index, but builds the (much smaller) reference index from the reference catalog. By running the *astrometry.net* client locally, an exposure with a few hundred to a thousand sources is typically solved within a fraction of a second.

The different matching techniques used by Scamp and *astrometry.net* complement each other for problematic fields. The disadvantages of the current implementation of *astrometry.net* (v0.43) include its inability to calculate relative photometric zero-points, while also offering little control over how e.g. distortion or chip alignment are handled, in particular for multi-chip cameras. *astrometry.net* calculates the distortion polynomial coefficients in the SIP convention (Shupe et al. 2012), which is not understood by SWarp which uses the older PV convention. Hence *astrometry.net* is currently used for catalog matching only, while Scamp is run automatically afterwards (with matching deactivated) to calculate the distortion maps and relative photometric zero-points.

### 6.3.3. *Shift and cross-correlation for mid-IR data*

Both `Scamp` and `astrometry.net` deliver full WCS solutions. However, they need sufficiently high object density to constrain all parameters. This is never the case for mid-IR data, where fields of view are (1) on the order of a few tens of arcseconds, and (2) contain only one or a few sources (possibly all non-stellar). In addition, suitable all-sky mid-IR catalogs with sufficient spatial resolution are not available. Thus for mid-IR data, THELI simply measures the linear shift between exposures in image coordinates, and constructs a dummy WCS solution that is understood by `SWarp` for stacking.

Two methods are available. In the first, the *Shift* approach is based on `SExtractor` catalogs and recommended for data in which one (or a few) point source(s) can be repeatedly detected in all images. Relative photometric zero-points are determined as well. In the second method, the offsets are determined using 2D cross-correlation of noise clipped images. This approach is recommended for data with predominantly extended flux. Relative photometry is *not* obtained, which is of little concern as mid-IR observations require clear and dry conditions. The WCS of the coadded images still has to be corrected manually, as global astrometry is not performed.

### 6.3.4. *Adopting the original WCS header*

If an astrometric solution cannot be found with either of the above methods, then the user can simply adopt the zero-order WCS solution already present in the raw FITS headers. Only `CRPIX1/2`, `CRVAL1/2` and the CD-matrix will be copied in this case, while distortion terms are ignored and relative photometric zero-points not calculated. This may be useful if the relative dither offsets between exposures are known to be precisely reflected in the headers.

### 6.3.5. *An astrometric challenge: AO images*

Current astrometric reference catalogs (e.g. USNO, 2MASS) are mostly based on plate scans or wide field images with an angular resolution on the order of  $1'' - 2''$ . This is about 3 – 5 times lower than the resolution of typical seeing-limited images, and does not pose a problem as long as fields are not very crowded. However, the limit is reached with adaptive optics (AO) systems such as GeMS/GSAOI@Gemini (McGregor et al. 2004), and similar instrumentation at future extremely large telescopes. The pixel scale

of GSAOI is  $0''.0197$ , 50 times smaller than the resolution element of the Digitized Sky Survey. Hence the source density of the plate scans becomes too low for successful catalog matching. Resolved multiple sources in the AO data introduce ambiguities, complicating the matching process further. The fields of view of current multi-conjugated AO (MCAO) systems are on the order of  $1'$ , and thus of the same size or smaller than many of the prominent science targets that will be revisited with these instruments. A global astrometric calibration of such data requires high resolution (and possibly much deeper) secondary catalogs obtained from images taken with 2m–8m class telescopes.

Figure 7 of globular cluster NGC 1851 illustrates the aforementioned challenges. The high source density in this field required a staggered approach. For the successful astrometry of the GSAOI data a tertiary catalog had to be used, obtained from a high resolution  $K_s$ -band HAWK-I@VLT image. This, in turn, could not be calibrated with USNO-B1 (no detections within the cluster) or 2MASS (too shallow in the outskirts, too few detections within the cluster). Instead, a reference catalog was extracted from an optical wide field image taken with WFI at the 2.2m MPG/ESO telescope, which itself was matched against 2MASS. At the other extreme we find observations of extragalactic targets, where hardly any reference sources are available in the common catalogs within a  $1'$  radius. Deep classical observations in good seeing are thus required to provide a secondary standard star catalog.

## 7. Sky subtraction

The main objective of sky subtraction is to achieve a homogeneous zero background level across the FP. At this point THELI assumes that any background variations are additive and hence must be subtracted, i.e. that the photometric zero-point is already uniform.

Sky subtraction is essential for multi-chip cameras. Consider two different pixels in a coadded image, constructed from  $n$  dithered exposures without sky subtraction. While all  $n$  exposures contribute to the first coadded pixel, the second pixel may lack data points due to detector gaps. If the background level varies between exposures, then their mean (or median) values at the position of the two coadded pixels will be different. Consequently, chip gaps will show up as discrete brighter or darker areas in the coadded image without prior sky subtraction.

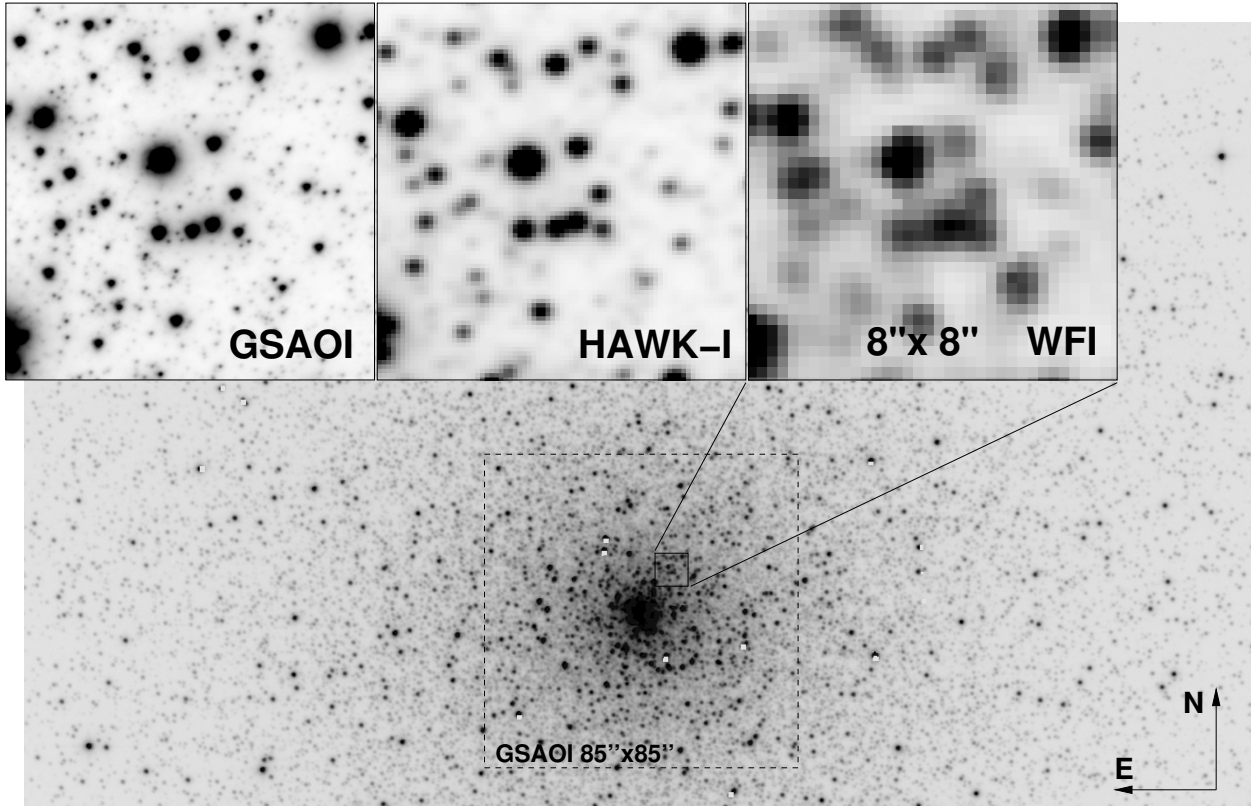


Fig. 7.— MCAO data pose a new challenge for astrometric calibration. Given the insufficient resolution of available reference catalogs, secondary or even tertiary catalogs are necessary (see text for details). The WFI/HAWK-I/GSAOI data in this example have a FWHM of  $0''.75$ ,  $0''.33$  and  $0''.08$ , and pixel scales of  $0''.24$ ,  $0''.10$  and  $0''.02$ , respectively. All data were reduced with THELI.

Difficulties arise for crowded fields or extended objects (with faint halos), where local and unbiased background measurements are difficult. Gradients caused by e.g. zodiacal light or the moon cause further complications. These can be controlled earlier on with separate sky exposures (see Sect. 4), and/or with the following two options for individual sky subtraction.

### 7.1. Full modeling

For sparse fields and fields without extended objects full background modeling can be done. The process is similar to what is described in E05, with some modifications. SExtractor is used to mask objects, with adjustable detection thresholds. To some degree a faint extended halo can be masked, as long as the amplitude of the background variations is smaller than that of the halo. The masked areas are interpolated iteratively, based on the values of non-masked pixels in the local

neighborhood. In this way background variations are reflected properly across larger masks, where a single constant estimate is insufficient. The resulting image, free of objects, is then convolved with a Gaussian kernel yielding the final sky model. Ideally, the kernel's FWHM is equal to or smaller than the typical extent of the background variations, yet large enough so that the filter remains insensitive to extended sources.

### 7.2. Subtracting a constant value

Background modeling on individual images is not an option whenever surface photometry or detection of faint extended structures is required. This holds in particular if the structures are not visible in individual images. Intra-cluster light, tidal features, and faint halos around brighter objects are good examples (Da Rocha et al. 2008; Tziamtzis et al. 2009; Martínez-Delgado et al. 2010; Guennou et al. 2012). To preserve the faint

structures a constant sky must be subtracted.

In THELI a constant background value can be determined individually for each chip of a detector mosaic, using various statistical estimators. Alternatively, a particular chip unaffected by the extended object can be used to estimate the sky level for all other chips. The measurement is performed either from the entire chip or from a sub-area, and after object masking has taken place (Sect. 7.1). Sub-areas can be defined using pixel coordinates (and are thus fixed to the detector), or by sky coordinates such that the measurement box moves with the dither pattern. The latter is useful for crowded fields, allowing the background to be measured repeatedly and precisely from the same location. Note that this (alternative) requires the *Update header* function to have been applied after the successful calculation of an astrometric solution (Sect. 6.3).

Should even more flexibility be required, the constant background values determined can be adjusted manually for individual chips or entire mosaics until the coaddition is satisfactory.

## 8. Coaddition

During the image coaddition phase the user can choose between the following SWarp parameters:

- Celestial coordinate systems (equatorial, galactic, ecliptic, supergalactic)
- WCS projections (TAN, COE, ...)
- Combine types (weighted mean, median, ...)
- Resampling kernels
- Output pixel scale

For multi-color data sets it is recommended to use identical reference coordinates (RA, DEC) for the sky projection. A particular object will then end up on precisely the same pixel in the coadded images of all different filters (see App. C.6). For non-equatorial coordinate systems the corresponding counterparts must be used, e.g. galactic longitude and latitude.

### 8.1. Filtering and arbitrary sky position angles

In the first step, SWarp gets a list of all images to stack, and creates a FITS header for the coadded image. At this level the user can decide which exposures enter the coaddition process, be it a selection by filter

(if a multi-color data set is present), seeing, and/or relative photometric zero-point. For multi-chip cameras a selection of chips can also be made, resulting in only part of the mosaic being created.

Two additional options act directly on the header of the coadded image before it is created. In case of wide-angle and all-sky projections it is difficult to predict the geometry of the coadded image, resulting in truncation. In this case the output size (NAXIS1/2) can be corrected. The other option is to choose an arbitrary sky position angle, as SWarp by default orients all stacked images with north up and east to the left. This is done by updating the CD-matrix, and increasing the image geometry to accommodate the new layout.

#### 8.1.1. Outlier rejection

In the second step, SWarp resamples the individual images, normally followed by the coaddition. SWarp does not however offer outlier rejection during stacking. While a median filter may be used to reject outliers during coaddition, its variance is a factor of  $\sim \pi/2$  higher compared to a mean combination (assuming Gaussian noise in the input images, see Sect. 3.13 of Kaiser 2002). The effective exposure time would need to be increased by a similar factor to compensate for this loss of sensitivity. THELI therefore offers the option of reconstructing the stacks for each coadded pixel based on the resampled images, identifying bad pixels by running a  $\sigma$ -clipping algorithm. Spurious pixels have then their weight set to zero in the resampled weight images. In this way photometric integrity is preserved while still using the weighted combination.

If a pixel is found to be bad, it may be masked only if the  $k$  neighboring pixels are also bad (*bad pixel cluster size*). This accounts for the fact that most resampling kernels distribute the flux of one input pixel over several output pixels. In addition, if a pixel is located  $m$  pixels or less from a bad pixel, it can also be masked. This is useful for the complete masking of bright asteroids or satellites, whose faint wings caused by the PSF go undetected by the outlier rejection.

#### 8.1.2. Locking onto proper motion targets

The proper motion vector of solar system objects can be projected into the headers of the resampled images, before final coaddition, by adjusting the CRVAL1/2 keywords. The coadded image then follows the moving target, whereas stars appear trailed. In this manner faint moving objects, possibly invisible in sin-

gle images, can be analyzed, provided their proper motions are known or can be guessed. The DATE-OBS keyword must be present in the input headers for sufficiently accurate timing. Currently, only linear proper motion vectors are supported, while second order effects are ignored. Figure 8 shows an example image.

### 8.1.3. Edge smoothing

In some cases it is not possible to achieve good sky subtraction, resulting in small discontinuous jumps at chip boundaries. This can be problematic for surface photometry or feature detection, in particular if the jump runs across the target. The discontinuity can be suppressed by *edge smoothing*, where the edges of the weight images are softened with a sine function of wavelength  $\lambda$  prior to resampling. Pixels at the outermost edge of the weight map are assigned a value of zero, corresponding to the minimum of the sine function. The pixel values then gradually increase inwards until they reach their original value after  $0.5\lambda$  (maximum of the sine function). Within this border the weight maps are unchanged. The 2nd derivatives at the transition points are zero. The chosen *edge smoothing length*,  $0.5\lambda$ , should be similar or a bit smaller than the size of the dither pattern. Photometry is conserved since this method is applied to the weight maps only. The noise level along the chip boundaries is increased by this process due to the lower weight.

## 9. Summary and outlook

In this paper I have presented an overview of the THELI data reduction pipeline. THELI integrates a large range of tools, and offers them in a homogeneous and convenient manner for end-to-end processing. Many different instruments at various observatories are pre-configured, and their data easily reduced. A short learning curve ensures quick success for new and more seasoned observers alike. The great flexibility facilitates a broad range of scientific studies, as demonstrated by e.g. Meech et al. (2005); Santander-García et al. (2008); Lieder et al. (2012); McMichael & Bentley (2012); Gentile et al. (2013) and Lane et al. (2013).

The development of THELI continues, as both astronomical instrumentation and software are highly dynamic areas. One of the main work areas, as already mentioned before, is a port to the newer Qt5 library ensuring cross-platform compatibility and the latest standard in GUI development. This next major release will

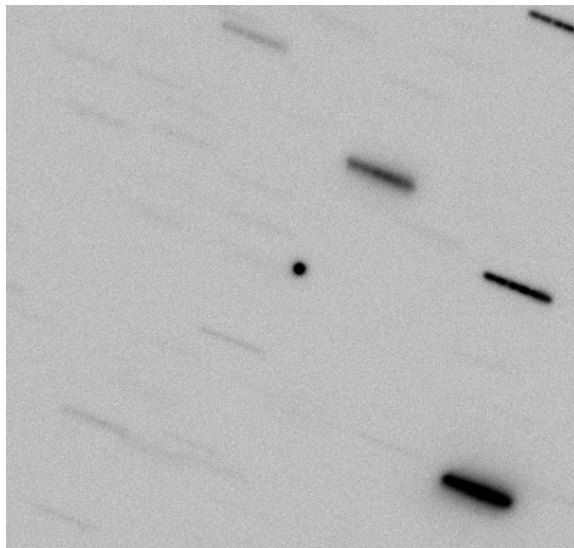


Fig. 8.— TNO 1996 TO<sub>66</sub>, as observed with FORS1@VLT using sidereal tracking (data from Sekiguchi et al. (2002)). The proper motion vector was applied during image coaddition.

also include automatic satellite detection and a method for 2D illumination correction (see Sect. 4). On the instrumental side, the focus is on mid-IR cameras and further support for instruments and observatories that are not yet included.

## Acknowledgements

I thank Douglas Applegate, Abdul Azim, Rafael Barrera, Yuri Beletsky, Albert Bosma, Andrew Cardwell, Cristiano daRocha, Matthias Frank, Javier Fuentes, Chon Gayoung, Karianne Holhjem, Richard Hook, Erik Kool, Andrea Kunder, Sean Lake, Richard Lane, Pierre Leisy, Stefan Lieder, Thorsten Lisker, Ed Loh, Grigoris Maravelias, Davide de Martin, James McCormac, Steffen Mieske, Oleg Maliy, Carsten Moos, Richard Müller, Felipe Navarete, Nadine Neumeyer, Daniela Olave Rojas, Emanuela Pompei, David Russell, Julia Scharwächter, Oliver Schütz, Zeinab Shafiee, Zahra Sheikhabahae, Tim Schrabback, Patrícia Figueiró Spinelli, Milan Stojanovic, Ignacio Toledo, Thomas Tuchan, Alex Tudorica, Daniela Wuttke, and Umut Yildiz for their numerous suggestions, testing, discussions, and access to data of new instruments. Their contributions resulted in the current functionality, support of many different instruments, and user friendliness of THELI. I apologize to all other

people who contributed their ideas and feature requests since 2004 and whose names I forgot. Special thanks goes to Thomas Erben for maintaining the THELI pipeline core, and to Emmanuel Bertin for his continuous development and support of SExtractor, SWarp and Scamp. Lastly, I would like to thank the anonymous referee for his very helpful comments about the manuscript, and Karianne Holhjem for substantial language editing.

## REFERENCES

- Ahn, C. P., Alexandroff, R., Allende Prieto, C., et al. 2012, *ApJS*, 203, 21
- Albert, L., Baril, M., Ward, J., Arnouts, S., & Devost, D. 2008, *Proc. SPIE*, 7014, 85
- Baade, D., Meisenheimer, K., Iwert, O., et al. 1999, *The Messenger*, 95, 15
- Banse, K., Crane, P., Grosbol, P., et al. 1983, *The Messenger*, 31, 26
- Beckett, M. G., Mackay, C. D., McMahon, R. G., et al. 1997, *Proc. SPIE*, 2871, 1152
- Bertin, E. 2006, in *ASP Conf. Ser.*, Vol. 351, ADASS XV, ed. C. Gabriel, C. Arviset, D. Ponz, & S. Enrique, 112
- Bertin, E. 2010, *Astrophysics Source Code Library*, 10068
- Bertin, E. & Arnouts, S. 1996, *A&AS*, 117, 393
- Butcher, H. & Stevens, R. 1981, *Kitt Peak National Observatory Newsletter*, 16, 6
- Crane, P., Rose, A., & Schabel, P. 1981, *Proc. SPIE*, 290, 120
- Cuillandre, J.-C., Luppino, G. A., Starr, B. M., & Isani, S. 2000, *Proc. SPIE*, 4008, 1010
- Cutri, R. M., Skrutskie, M. F., van Dyk, S., et al. 2003, *2MASS All Sky Catalog of point sources*. (CDS)
- Da Rocha, C., Ziegler, B. L., & Mendes de Oliveira, C. 2008, *MNRAS*, 388, 1433
- Erben, T., Hildebrandt, H., Miller, L., et al. 2013, *MNRAS*, 433, 2545
- Erben, T., Schirmer, M., Dietrich, J., et al. 2005, *AN*, 326, 432
- Flaugher, B. L., Abbott, T. M. C., Angstadt, R., et al. 2012, *Proc. SPIE*, 8446, 11
- Freyhammer, L. M., Andersen, M. I., Arentoft, T., Sterken, C., & Nørregaard, P. 2001, *Experimental Astronomy*, 12, 147
- Gentile, G., Józsa, G. I. G., Serra, P., et al. 2013, *A&A*, 554, A125
- Goad, L. E. & Ball, W. F. 1981, *Proc. SPIE*, 290, 130
- Guennou, L., Adami, C., Da Rocha, C., et al. 2012, *A&A*, 537, A64
- Gunn, J. E. & Westphal, J. A. 1981, *Proc. SPIE*, 290, 16
- Heymans, C., Van Waerbeke, L., Miller, L., et al. 2012, *MNRAS*, 427, 146
- Hildebrandt, H., Erben, T., Dietrich, J. P., et al. 2006, *A&A*, 452, 1121
- Hummel, W., Hanuschik, R., de Bilbao, L., et al. 2010, *Proc. SPIE*, 7737, 35
- Hunt, L. K., Mannucci, F., Testi, L., et al. 1998, *AJ*, 115, 2594
- Ivezić, Ž., Smith, J. A., Miknaitis, G., et al. 2007, *AJ*, 134, 973
- Jacoby, G. H., Tonry, J. L., Burke, B. E., et al. 2002, *Proc. SPIE*, 4836, 217
- Kaiser, N. 2002, *Elements of Astrophysics* (University of Hawaii, available online at <http://www.ifa.hawaii.edu/~kaiser/lectures/elements.pdf>)
- Kaiser, N., Wilson, G., Luppino, G., & Dahle, H. 1999, preprint astro-ph/9907229
- Koch, A., Odenkirchen, M., Grebel, E. K., & Caldwell, J. A. R. 2004, *Astronomische Nachrichten*, 325, 299
- Kuijken, K., Bender, R., Cappellaro, E., et al. 2002, *The Messenger*, 110, 15
- Landolt, A. U. 1992, *AJ*, 104, 340
- Lane, R. R., Salinas, R., & Richtler, T. 2013, *A&A*, 549, A148

- Lang, D., Hogg, D. W., Mierle, K., Blanton, M., & Roweis, S. 2010, *AJ*, 139, 1782
- Lasker, B. M., Lattanzi, M. G., McLean, B. J., et al. 2008, *AJ*, 136, 735
- Leggett, S. K., Currie, M. J., Varricatt, W. P., et al. 2006, *MNRAS*, 373, 781
- Leggett, S. K., Hawarden, T. G., Currie, M. J., et al. 2003, *MNRAS*, 345, 144
- Lieder, S., Lisker, T., Hilker, M., Misgeld, I., & Durrell, P. 2012, *A&A*, 538, A69
- Magnier, G. & Cuillandre, J.-C. 2004, *PASP*, 116, 449
- Manfroid, J., Selman, F., & Jones, H. 2001, *The Messenger*, 104, 16
- Martínez-Delgado, D., Gabany, R. J., Crawford, K., et al. 2010, *AJ*, 140, 962
- McGregor, P., Hart, J., Stevanovic, D., et al. 2004, *Proc. SPIE*, 5492, 1033
- McLean, I. S., Cormack, W. A., Herd, J. T., & Aspin, C. 1981, *Proc. SPIE*, 290, 155
- McMichael, R. T. & Bentley, J. 2012, *Proc. SPIE*, 8486, 2
- Meech, K. J., Ageorges, N., A'Hearn, M. F., et al. 2005, *Science*, 310, 265
- Miyazaki, S., Komiyama, Y., Nakaya, H., et al. 2012, *Proc. SPIE*, 8446, 0
- Miyazaki, S., Komiyama, Y., Sekiguchi, M., et al. 2002, *PASJ*, 54, 833
- Monet, D. G., Levine, S. E., Canzian, B., et al. 2003, *AJ*, 125, 984
- Mortara, L. & Fowler, A. 1981, *Proc. SPIE*, 290, 28
- Nikolaev, S., Weinberg, M. D., Skrutskie, M. F., et al. 2000, *AJ*, 120, 3340
- Onaka, P., Tonry, J. L., Isani, S., et al. 2008, *Proc. SPIE*, 7014, 12
- Pavelin, C. J. & Walter, A. J. H. 1980, *Proc. SPIE*, 264, 70
- Peña Ramírez, K., Zapatero Osorio, M. R., Béjar, V. J. S., Rebolo, R., & Bihain, G. 2011, *A&A*, 532, A42
- Perryman, M. A. C. & ESA, eds. 1997, *ESA Special Publication*, Vol. 1200, *The HIPPARCOS and TYCHO catalogues. Astrometric and photometric star catalogues derived from the ESA HIPPARCOS Space Astrometry Mission*, ed. M. A. C. Perryman & ESA
- Persson, S. E., Murphy, D. C., Krzeminski, W., Roth, M., & Rieke, M. J. 1998, *AJ*, 116, 2475
- Roeser, S., Demleitner, M., & Schilbach, E. 2010, *AJ*, 139, 2440
- Santander-García, M., Corradi, R. L. M., Mampaso, A., et al. 2008, *A&A*, 485, 117
- Schirmer, M., Erben, T., Schneider, P., et al. 2003, *A&A*, 407, 869
- Schirmer, M., Hildebrandt, H., Kuijken, K., & Erben, T. 2011, *A&A*, 532, 57
- Sekiguchi, T., Boehnhardt, H., Hainaut, O. R., & Delahodde, C. E. 2002, *A&A*, 385, 281
- Shupe, D. L., Laher, R. R., Storrie-Lombardi, L., et al. 2012, *Proc. SPIE*, 8451, 1
- Skrutskie, M. F., Cutri, R. M., Stiening, R., et al. 2006, *AJ*, 131, 1163
- Smith, J. A., Tucker, D. L., Allam, S. S., et al. 2007, in *ASP Conf. Ser.*, Vol. 364, *The Future of Photometric, Spectrophotometric and Polarimetric Standardization*, ed. C. Sterken, 91
- Stetson, P. B. 2000, *PASP*, 112, 925
- Tziamtzis, A., Schirmer, M., Lundqvist, P., & Sollerman, J. 2009, *A&A*, 497, 167
- Uchimoto, Y. K., Yamada, T., Kajisawa, M., et al. 2012, *ApJ*, 750, 116
- Valdes, F. 1984, in *Bulletin of the American Astronomical Society*, Vol. 16, *Bulletin of the American Astronomical Society*, 497
- von der Linden, A., Allen, M. T., Applegate, D. E., et al. 2012, *ArXiv e-prints*
- Zacharias, N., Finch, C. T., Girard, T. M., et al. 2012, *VizieR Online Data Catalog*, 1322, 0

---

This 2-column preprint was prepared with the AAS L<sup>A</sup>T<sub>E</sub>X macros v5.2.

Online material

## A. Optical example: VLT/FORS1

This section introduces the basic reduction steps with THELI, using a set of raw data taken from the ESO archive<sup>8</sup>. The idea is to provide the beginner with a simple data set and a sense for how THELI works. Only mandatory steps are covered, i.e. preparation of the data, the main calibration, weighting, astrometry, sky subtraction and coaddition. The example is based on the small *R*-band FORS1@VLT data set listed in Table 1 and taken by Sekiguchi et al. (2002), for TNO 1996 TO<sub>66</sub> (Fig. 8). At that time FORS1 was a single-chip camera. Treatment of multi-chip data is identical, with one exception occurring during astrometry (highlighted in App. /refexample2).

Table 1: Small FORS1@VLT data set for the example in App. A. Exposures can be identified in the ESO raw science archive by selecting FORS1 as instrument, entering “13 11 1999” for the night, and by limiting the maximum number of output rows to 200.

File name
BIAS
FORS.1999-11-14T11:35:16.454.fits
FORS.1999-11-14T11:36:02.607.fits
FORS.1999-11-14T11:36:49.109.fits
FORS.1999-11-14T11:37:35.510.fits
FORS.1999-11-14T11:38:22.303.fits
FLAT
FORS.1999-11-13T23:42:09.117.fits
FORS.1999-11-13T23:43:21.663.fits
FORS.1999-11-13T23:44:40.835.fits
FORS.1999-11-14T09:17:20.006.fits
FORS.1999-11-14T09:18:14.457.fits
SCIENCE
FORS.1999-11-14T00:26:52.043.fits
FORS.1999-11-14T00:38:56.322.fits
FORS.1999-11-14T00:51:18.793.fits
FORS.1999-11-14T01:03:58.970.fits
FORS.1999-11-14T01:16:04.471.fits
FORS.1999-11-14T01:28:27.545.fits
FORS.1999-11-14T01:45:35.796.fits
FORS.1999-11-14T01:57:40.224.fits
FORS.1999-11-14T02:10:04.102.fits
FORS.1999-11-14T02:27:48.341.fits

<sup>8</sup>[http://archive.eso.org/eso/eso\\_archive\\_main.html](http://archive.eso.org/eso/eso_archive_main.html)

## A.1. Initializing THELI and preparing the data

Sort the uncompressed data into three arbitrarily named sub-directories BIAS, FLAT and SCIENCE, which share the same parent directory, /MAINPATH. Next, in THELI’s *Initialise* section,

- enter a project name (e.g. FORS1\_DEMO)
- select the number of CPUs you want to use
- select FORS1\_1CCD@VLT from the instrument list
- let THELI know the directory tree (Fig. 1).

In the *Preparation* section, mark the *Split FITS / correct header* task and launch it by clicking on *Start*. THELI will cycle through the three data directories, split multi-extension FITS files into single FITS files (if applicable), and translates the FITS headers (Sect. 3.1). File names will end in *\_i.fits*, where *i* will run from 1 to *n* for a multi-chip camera with *n* detectors.

## A.2. Calibration

Mark *Process biases*, *Process flats* and *Calibrate data*. This creates the master bias and the bias-corrected master flat, /MAINPATH/BIAS/BIAS\_1.fits, /MAINPATH/FLAT/FLAT\_1.fits, and applies both to the science data. All files are also overscan corrected and trimmed. The tasks can be executed individually or in one go. File names in SCIENCE will now end in *\_1OFC.fits*, where the status string OFC indicates that the exposures have run through this pre-processing stage. Other steps at a later stage, such as background modeling, append more characters to the status string, but they are not required here.

## A.3. Weighting

The global weight is a copy of the normalized flat field, where static bad pixels can optionally be zeroed (Sect. 5). It forms the basis for the individual weight maps. All weight images can be found in /MAINDIR/WEIGHTS.

Mark *Create global weights* and *Create WEIGHTS* and run both tasks with their default configuration settings. The global weight maps should be inspected for excessive masking if tighter lower and upper thresholds are chosen for the normalized flat.

#### A.4. Astrometry and relative photometry

First, we need to download the astrometric reference catalog. Select SDSS-DR9 and a magnitude limit of 23, so we get sufficiently many sources matching the VLT data. The search radius is automatically adjusted to 5'. Click on *Get catalog* to download nearly 500 reference sources. Then run *Create source cat* with its default parameters, which creates the binary catalogs for each exposure in `/MAINPATH/SCIENCE/cat`. Therein you will also find `ds9cat` and `skycat` sub-directories, containing catalogs formatted for overlay in these two FITS viewing programs. Two versions of the astrometric reference catalog, called `ds9cat/theli_mystd.reg` and `skycat/theli_mystd.skycat`, are kept there as well.

Now run the astrometry. Mark *Astro+photometry*, select *Scamp* from the pull-down menu next to the task, and click on *Configure*. The default settings work with a broad range of data. Click on *Defaults (this page)* to make sure no different values from a previous run are loaded. Close the configuration dialog, and start the astrometry task. Once done, the sub-directory `/MAINPATH/SCIENCE/plots` contains the *Scamp* check plots which you should inspect<sup>9</sup>. The most important ones are

- `fgroups_1.png`: The exposures' layout on sky. Green (red) marks indicate objects in the reference catalog that were (not) matched by an object in the exposures. You should recognize the dither pattern. The image frames displayed should not appear sheared or distorted, and you should recognize the dither pattern.
- `distort_1.png`: The optical distortion, encoded as a change of pixel scale across the field. This should be circularly symmetric and aligned with the optical axis of the telescope (usually at the center of the detector array).
- `astr_referror_1.png`: The astrometric residuals with respect to the reference catalog. No systematic trends should be visible, and the scattering should represent the astrometric uncertainties of the reference catalog.
- `astr_interror_1.png`: The internal astrometric residuals, i.e. the accuracy exposures were

<sup>9</sup>A large selection of good and bad *Scamp* check plots is shown in the online user manual.

registered with respect to each other. This should be on the order of 1/5th to 1/15th of a pixel, and systematic trends should be absent.

#### A.5. Sky subtraction and coaddition

No extended sources are present, therefore normal sky modeling is adequate. In the *Coaddition* section, enter the configuration for sky subtraction, select *Model the sky* and load the default parameters. Exit the dialog, mark and run the *Sky subtraction* task. The names of the sky-subtracted images end in `_10FC.sub.fits`.

Lastly, perform the image coaddition with the default parameter configuration. If you want, enter a proper motion vector of  $\Delta RA = -1''.531915 \text{ hr}^{-1}$  and  $\Delta DEC = -0''.59283 \text{ hr}^{-1}$  to register the exposures on the TNO, reproducing Fig. 8. Enter an extra *Identification string* so that a previous coaddition without proper motion is not overwritten. Exit the configuration dialog and run the task. The final coadded image and weight can be found in `SCIENCE/coadd_<ID>/coadd.[weight].fits`, where `<ID>` is either the filter in which the images were taken, or a user-supplied identifier.

## B. Near-IR example: HAWK-I@VLT

This example is based on *H*-band observations of low mass objects in the  $\sigma$  Orionis cluster (Peña Ramírez et al. 2011). The necessary reduction steps for near-IR data are shown, focussing on the background modeling. The latter can be configured in many different ways, hence only the settings relevant for this data set are explained. Since HAWK-I@VLT consists of 4 HAWAII-2 detectors, this example also explains how astrometry is achieved for mosaic cameras. Settings already explained in App. A are not repeated here unless their importance is to be emphasized.

### B.1. Initializing THELI and preparing the data

Sort the uncompressed data into sub-directories `FLAT`, `FLAT_OFF` and `SCIENCE`, sharing the same parent directory, `MAINPATH`. Choose a new project name, e.g. `HAWKI_DEMO`, select `HAWKI@VLT` in the instrument list, and make the directory tree known to THELI.

In the *Preparation* section, mark the *Split FITS / correct header* task. This time file names will end in `_i.fits`, where `i` runs from 1 to 4, representing the four chips of HAWK-I.

Table 2: HAWK-I@VLT data for the example in App. B. The flats can be located in the ESO raw science archive by entering “08 12 2008” for the night, *H* for the filter, and FLAT for the data type. For the science exposures (abridged) choose “07 12 2008”, select *H* for the filter, and OBJECT for the data type.

File name
FLAT
HAWKI.2008-12-08T23:42:44.267.fits
HAWKI.2008-12-08T23:42:56.627.fits
HAWKI.2008-12-08T23:43:08.978.fits
HAWKI.2008-12-08T23:43:21.381.fits
HAWKI.2008-12-08T23:43:33.738.fits
HAWKI.2008-12-08T23:43:46.669.fits
HAWKI.2008-12-08T23:43:59.023.fits
FLAT_OFF
HAWKI.2008-12-08T23:52:04.524.fits
HAWKI.2008-12-08T23:52:14.233.fits
HAWKI.2008-12-08T23:52:26.606.fits
HAWKI.2008-12-08T23:52:38.957.fits
HAWKI.2008-12-08T23:52:51.921.fits
HAWKI.2008-12-08T23:53:04.321.fits
HAWKI.2008-12-08T23:53:17.273.fits
SCIENCE
HAWKI.2008-12-08T04:40:22.699.fits
HAWKI.2008-12-08T04:42:54.715.fits
HAWKI.2008-12-08T04:45:28.151.fits
HAWKI.2008-12-08T04:48:01.630.fits
[...]
HAWKI.2008-12-08T05:44:19.241.fits
HAWKI.2008-12-08T05:46:52.674.fits
HAWKI.2008-12-08T05:49:26.152.fits
HAWKI.2008-12-08T05:51:59.587.fits

## B.2. Calibration

First, set the *Do not apply BIAS / DARK* check box as the pre-read is already subtracted from near-IR data<sup>10</sup>. Run *Process flats* to create combined bright and dark flats. The bright flat will have the dark flat subtracted automatically. If you do not want to subtract a dark flat, just do not provide that data. Next, run *Calibrate data* to apply the flat field to the science images.

<sup>10</sup>If you want to subtract a dark, remove this setting after the master flat was created, and select *Use dark* next to the *Calibrate data* task.

## B.3. Background modeling

Now a background model has to be removed, a task inevitable with near-IR data. This is done in the *Background* section. First of all, we have to decide whether we want a one-pass or a two-pass background model. In most cases a two-pass approach is required, unless the field is empty, exposures were frequently and widely dithered, and / or accurate photometry is not necessary. Our field has several bright stars and may contain nebosity. A two-pass strategy is therefore adequate, meaning the same task is run twice, the second time with fine-tuned parameters.

### B.3.1. First pass of the background model

Open the configuration for *Background model correction*. You will be presented with the following settings.

1. **Mask objects:** For the first pass, remove the default entries for DT and DMIN, representing the SExtractor DETECT.THRESH and DETECT.MINAREA parameters. This will create a quick and simple background model without prior object masking<sup>11</sup>. Select the *Median* combination, and switch *off* the SExtractor filtering.
2. **Reject pixels from the stack:** By default, the highest pixel in the stack is rejected prior to stack combination. Accept this setting. You may want to increase this number if you create larger static stacks, have high source density, and / or larger dynamic window sizes.
3. **How to apply the background model:** Different options are available. For near-IR data we *subtract* the model and leave the two smoothing scales empty. We want to *rescale* the model to take out any temporal global intensity variations. We do not apply the model to SKY data (because we do not have SKY exposures in this example), and we also do not adjust the gains between chips (done during flat-fielding).
4. **Static or dynamic model:** Choose a *window size* of 6, and accept the default value for the maximum gap size (1.0h; there is no gap in

<sup>11</sup>If you want object masking at this stage, e.g. because a two-pass is not necessary, choose DT and DMIN high enough such that no background features will be masked, e.g. DT=20, DMIN=10.

this exposure sequence if the same exposures as listed in Table 2 are used).

Once finished, the files will have the string OFCB in their names. The previous OFC images are parked in OFC\_IMAGES, and a MASK\_IMAGES sub-directory contains the object masks from which the background model was calculated. Since we chose to not detect objects, the masks are simply links to the unmasked data. The background models for each individual image can be found in the BACKGROUND directory.

In case horizontal or vertical gradients from a reset anomaly are still present (as in Fig. 4), one should now run the *Collapse correction* task (Sect. 4.2). This is not necessary for the present data.

### B.3.2. Second pass of the background model

At this point the images are mostly flat, revealing fainter objects (which can thus be masked). To create an improved background model we simply repeat the task with modified parameters  $DT=1.5$  and  $DMIN=10$ .

THELI will recognize that this is the second pass. Objects detected in the OFCB images will be masked in the OFC images (parked in OFC\_IMAGES), and the improved masks can be found again under MASK\_IMAGES. The temporary OFCB images from the 1st pass will be moved to OFCB\_IMAGES\_1PASS, and the original OFC images are restored. Improved background models are calculated and applied, resulting in the final set of OFCB images.

Inspect a few of the masks and the resulting OFCB exposures, in particular a few at the beginning, the middle and at the end of the sequence. Relax  $DT=1.5$  if excessive masking is recognized, and simply re-run the task. In general, two passes are sufficient. One without any detection thresholds (faster), and the second one with correctly chosen settings. If necessary, a collapse correction can be applied afterwards.

### B.3.3. Separate sky exposures

If extended sources were present in these HAWK-I data, then the background model could not be calculated from the data themselves. Instead, separate exposures of a nearby blank field would be needed. They have to be collected in a SKY directory (Sect. 4.1.1), where THELI would find and automatically process them. This is not the case for this example, but I include it here as it is a common procedure.

In the following, the letter 'O' denotes an object exposure, and the letter 'S' a sky exposure. For example, alternating sequences could be

- 00000-SSSSS
- 000-SSS-000-SSS- . . .
- 00-S-00-S-00-S- . . .

The first one would be chosen for a short observation of a brighter target, justifying a static background model. The other sequences could also be processed with a single static model, but the layout suggests that the observer wanted to keep track of the sky variations, calling for a dynamic model. The layout of the sequences *does not matter* to THELI. You simply collect all sky exposures in a separate SKY directory. For the dynamic model, THELI will identify the closest sky exposures in time for a given object exposure, based on the window size, and assuming that a valid (modified) Julian date MJD-OBS is present in the FITS headers. The latter should be the case for all pre-defined instruments in THELI, but you may want to check, as the raw FITS headers may have changed or be corrupted.

## B.4. Weighting

Weighting is essentially the same as for optical data. Tighter thresholds should be chosen for the normalized flat to remove spurious pixel clusters. Set the min and max values for FLAT\_norm to 0.9 and 1.1, respectively, and check the WEIGHT/globalweight.i.fits images for excessive masking.

## B.5. Astrometry and relative photometry

For the reference catalog we choose again SDSS-DR9 and a magnitude limit of 23, which will result in about 800 reference sources. For a field with high extinction 2MASS could be a better choice to maximize the overlap between reference and source catalogs. *Create source cat* can be run with its default parameters. For sparser fields than this example, DT can be lowered from 5 to about 1.5 to get sufficiently many objects.

Use Scamp for the astrometry, and select the default configuration parameters as for the first example. However, set MOSAIC.TYPE = SAME\_CRVAL as we are processing data from a multi-chip camera. A focal plane (FP) model that has been determined previously based on observations of a dense stellar field will then form the basis of the final astrometric solution. This

covers relative chip positions and rotations, as well as the CD-matrix<sup>12</sup>. Even sparse fields with only few detections per chip can thus be solved. A prior distortion model, however, cannot be loaded by current versions of *Scamp*. The distortion is determined by *Scamp* from the dithered data themselves.

All pre-configured multi-chip instruments in THELI have their FPs already determined in this manner. It may happen that these default FPs need to be updated, e.g. after a dead detector has been replaced, the optics re-aligned, or if the quality of the astrometric solution is insufficient. In these cases you can create a new FP from a different stellar field taken more recently, or simply from the current data set itself. To create a new FP, set `FOCAL_PLANE = Create new FP`, otherwise leave the default setting `Use default FP`.

### B.6. Sky subtraction and coaddition

In Sect. B.3 a dynamic background model was subtracted. Yet small constant non-zero offsets on the order of half a percent of the original background level may still be present in the images, together with spatial variations of similar amplitude if the atmosphere was particularly unstable. Running an individual sky background model as shown for the optical example suppresses these residuals to a level of  $\sim 0.1\%$  or less. Alternatively, you can choose a constant sky subtraction.

The coaddition can be performed with default parameters.

## C. Mid-IR example: T-ReCS@GEMINI

This example is based on multi-band observations of the circum-nuclear starburst ring in NGC 7552, (Table C; PI B. Rodgers), and shown in Fig. 5. The data can be obtained from the Gemini Science Archive. T-ReCS is a highly sensitive mid-IR imaging spectrograph and was offered at Gemini-South until 2012. This example highlights the typical chop-nod process for ground-based mid-IR observations, the special requirements for astrometry, and THELI's general support for multi-color data sets during coaddition.

<sup>12</sup>The prior CD-matrix will override the CD-matrix values from the FITS headers. If the position angle of your observations is different from the FP by more than `POSANGLE_MAXERR`, then the matching with the reference catalog will fail. Simply set `POSANGLE_MAXERR = 180` to allow for all position angles to be searched.

Table 3: Multi-band T-ReCS@GEMINI data for the mid-IR example in Appendix C. The exposures can be found in the Gemini Science Archive, by entering NGC 7552 for the object, and T-ReCS for the instrument.

File name	Bandpass
S20110722S0134.fits	[Si II] 8.8 $\mu$ m
S20110722S0135.fits	[Si II] 8.8 $\mu$ m
S20110722S0136.fits	[Ne II] 12.8 $\mu$ m
S20110722S0137.fits	[Ne II] 12.8 $\mu$ m
S20110722S0138.fits	[Ne II] 13.1 $\mu$ m
S20110722S0139.fits	[Ne II] 13.1 $\mu$ m
S20110726S0086.fits	Qa 18.3 $\mu$ m
S20110726S0087.fits	Qa 18.3 $\mu$ m

### C.1. Initializing THELI and preparing the data

T-ReCS images (and those of other mid-IR cameras) are usually not flat fielded due to the highly variable mid-IR background. Likewise, a bias or dark subtraction is unnecessary as it is taken care of automatically by the pairwise image subtraction. Therefore, all images listed in Table 3 may be copied into the same SCIENCE directory. Choose a new project name, e.g. `NGC7552_MIR`, select `TRECS@GEMINI`, and make the directory tree known to THELI.

In the *Preparation* section, mark the *Split FITS / correct header* task, and check the *Split MIR cubes* option. Contrary to optical and near-IR data, several additional processing steps take place for T-ReCS. First, THELI checks whether the images were taken in full chop-nod mode, which is the case for almost all exposures with T-ReCS (and currently the only supported mode for this camera). The images used in this example typically contain 8 – 9 extensions with a full chop-nod cycle. THELI will perform the chop-nod sky subtraction and write out separate images per cycle, as we asked to split the cubes. If the target was very faint and only visible in the stacked cube, then the splitting option should not be checked, as otherwise the astrometry will become unfeasible.

### C.2. Calibration

As mentioned above, no dark or flat correction is done. Most of the sky and telescope background was already removed in the previous step. Nevertheless, the calibration task has to be run for compatibility reasons, otherwise the data will not propagate properly through THELI. Simply set the *Do not apply BIAS /*

*DARK* and *Do not apply FLAT* check boxes, and run *Calibrate data*. The latter will merely insert the standard OFC string into the file names, and set some internal processing flags.

### C.3. Collapse correction

The chop-nod background correction for mid-IR depends strongly on the atmosphere's precipitable water vapor and possible cirrus. Observations are only possible in dry and clear conditions, in particular in the *Q* bandpass centered on  $20\mu\text{m}$ . Chop-nod cycles taken in unstable conditions may show strong background residuals and should be discarded. This is why THELI does not automatically combine all cycles during splitting, but leaves them for individual inspection so that bad exposures can be discarded manually.

For this example data set no images have to be rejected. However, you may notice that a small vertical gradient exists in some of the data. This can be easily corrected for using the *Collapse correction*. Adopt the default configuration values (leave *DT* and *DMIN* empty), with *x* as the collapse correction. We want to exclude the entire extended and diffuse object from the modeling, defining the vertices of the excluded region as *xmin=110*, *xmax=220*, *ymin=50*, and *ymax=160*. This is for the [Si II]  $8.8\mu\text{m}$ , [Ne II]  $12.8\mu\text{m}$ , and [Ne II]  $13.1\mu\text{m}$  filters. The observations in the *Qa*  $18.3\mu\text{m}$  bandpass are significantly offset and require *xmin=130*, *xmax=240*, *ymin=70*, and *ymax=180*. To achieve this, park the *Qa* exposures in a temporary directory and run the collapse correction with the first setting on the [Si II] and [Ne II] exposures. Then exchange the images in the current and the temporary directory, and apply the collapse correction to the *Qa* exposures with the updated exclusion region. After that, merge all images again in the *SCIENCE* directory.

### C.4. Weighting

As no flat field is available, the individual weights are based on constant global weights with value unity. Select *Same weight for all pixels* in the configuration of *Create global weights*. The individual weights can be created with default settings, i.e. cosmics, hot pixels and obvious static pixel defects will be masked.

### C.5. Astrometry and photometry

Mid-IR images probe a vastly different part of the spectrum than optical or near-IR images, and typically

only one or two compact sources or diffuse emission are seen. Matching with common astrometric reference catalogs, a full distortion correction and/or WCS solution is in general not possible. Usually, a simple linear registration of images is sufficient. The global WCS in the final coadded image will be limited by the accuracy of the WCS in the FITS raw data, and may have to be adjusted by hand if necessary.

Two possibilities exist for mid-IR data. In case of a single point source, the simple *Shift (float)* approach can be used, requiring the creation of source catalogs as discussed in the previous examples. This approach does not work here, as one or several point sources may be detected in the individual images, together with extended flux. The number of sources is very small, and hence an unambiguous cross-identification of exposures is unlikely. Imagine you have one image with one source detected, and another one with two sources. Without further prior information, such as assumptions about the accuracy of the WCS in the header, it is not possible to register these two images automatically. Use the cross-correlation method (*Xcorr*) instead. It will run *SExtractor* with fixed low detection thresholds to create images containing compact and extended source flux only. These are then cross-correlated, yielding the relative offsets.

### C.6. Sky subtraction and coaddition

After *collapse correction* the mean sky background level is zero, therefore sky subtraction can be skipped. If the collapse correction was not done, the images may still show some constant offset which can be removed using the *Mode* in *Subtract a constant sky*.

Coaddition is performed with default settings. However, since we have observations in 4 different bands present in the same directory, we want the final coadded images to have identical geometries. We also want the same physical object to appear in the same pixel. This is achieved as follows:

1. First, find the RA and DEC values of the center of your image. It does not need to be accurate, but if you are too far off, the coadded image could be truncated. Enter these values as *Ref RA|DEC* in the configuration of the *Coaddition* dialog. For this example we use *RA=23:16:10.6* and *DEC=-42:35:04*. By using the same values for the coadditions of all 4 bands, we enforce an identical astrometric de-projection needed for automatic image registra-

tion later on.

2. *Coadd this filter:* In this pull-down menu THELI presents a list of the 4 bands available in the SCIENCE directory. Start with the first one, NeII-12.8um, which will create a coadd\_NeII-12.8um directory containing the corresponding coadded image.
3. Optionally, you can choose an additional outlier rejection by setting `threshold=3` and `cluster size=4`

At this point, four `coadd.<filter>` directories are present, with the stacked images and their weights, `coadd.[weight].fits`. While these have identical values of `CRVAL` and `CRPIX`, their geometries are still different due to initial pointing variations, chop-nod offsets etc. To register the images, go to the main menu at the top of the THELI window, and open *Miscellaneous* → *Prepare color picture*. You will be presented with a list of all `coadd.<filter>` directories. Select the ones you are interested in, and then click on *Get coadded images*. This will create a `SCIENCE/color_theli` directory, containing the coadded images registered and trimmed to their maximum common overlap, and called `<filter>_cropped.[weight].fits`. Note that since THELI enforces integer values for the `CRPIX` header keywords during coaddition, excess pixels can simply be removed and no second resampling has to take place that would degrade image quality.

This approach works for any other multi-color data set. The only requirement is that identical reference RA and DEC values are used for the coadditions of the different bands, and that the final `coadd.<ID>` directories are collected in the same SCIENCE directory.

#### **D. Currently supported instruments**

Table 4: Pre-configured optical imagers

Instrument@Telescope	# detectors	Comment
ACAM@WHT	1	
ALFOSC@NOT	1	
ALTAU16M@VYSOS06	1	
AltaU42@ASV	1	Low and high resolution modes
CFH12K@CFHT	12	Before and after detector swap in September 1999
DECam@CTIO	62	
EFOSC2@ESO3.6m	1	1 × 1 and 2 × 2 binning
EMMI@NTT	1	BIMG and RILD imaging modes
ENZIAN_CAS@HOLI_1M	1	
FORS1@VLT	1	old and new configuration with 1 and 2 CCDs, respectively
FORS2@VLT	1	old and new configuration with 1 and 2 CCDs, respectively
GMOS@GEMINI-NORTH	3	1 × 1 and 2 × 2 binning
GMOS@GEMINI-SOUTH	3	1 × 1 and 2 × 2 binning
GOODMAN@SOAR	1	1 × 1 and 2 × 2 binning
GPC1@PS1	64	
GROND_OIMG@MPGESO	1	
IMACS_F2@LCO	8	old and new detector configuration
IMACS_F4@LCO	8	old and new detector configuration
LAICA_2x2@CAHA	4	1 × 1 and 2 × 2 binning
LBC@LBT	4	BLUE and RED cameras
LDSS3@LCO	2	
LORRI@NewHorizons	1	
MEGACAM@LCO	36	2 × 2 binning only
MEGAPRIME@CFHT	36	Support for raw and ELIXIR pre-processed data
MEROPE@MERCATOR	1	
MOSAIC-I@KPNO_0.9m	8	Old configuration (before Aug. 2010)
MOSAIC-I@KPNO_4.0m	8	Old configuration (before Aug. 2010)
MOSAIC-II@CTIO	8	8- and 16-channel mode, before and after fix of dead readout port
MOSCA_2x2@NOT	4	2 × 2 binning only
OASIS4x4@WHT	1	1 × 1 and 4 × 4 binning
OMEGACAM@VST	32	
PFC@WHT	2	
SDSS	1	For SDSS images directly downloaded from the server
SOI@SOAR	2	
SuprimeCam_OLD@SUBARU	10	Before and after April 2001 (replacement of dead CCD)
SuprimeCam_NEW@SUBARU	10	Installed August 2008; Support for raw and SDFRED pre-processed data
SuSI2_2x2@NTT	2	2 × 2 binning only
VIMOS@VLT	4	
WFC@INT	4	1 × 1 and 2 × 2 binning
WFI@AAT	8	
WFI@SSO_40inch	7	
WFI@MPGESO	8	
Y4KCam@CTIO	1	

Table 5: Pre-configured near- and mid-IR imagers

Instrument@Telescope	# detectors	Comment
FLAMINGOS2@GEMINI-SOUTH	1	
FourStar@LCO	4	
GROND_IRIM@MPGESO	1	
GSAOI@GEMINI-SOUTH	4	
HAWKI@VLT	4	
INGRID@WHT	1	
ISAAC@VLT	1	
LIRIS@WHT	1	Normal imaging and polarimetry mode
MMIRS@LCO	1	
MOIRCS@SUBARU	4	
NACOSDI@VLT	1	
NEWFIRM@CTIO	4	
NICS@TNG	1	
NICI@GEMINI-SOUTH	2	
NIRI@GEMINI-NORTH	1	
NOTcam@NOT	1	High and low resolution modes
Omega2000@CAHA	1	
OSIRIS@SOAR	1	High and low resolution modes
OSIRIS@GTC	1	
PISCES@LBT	1	
SOFI@NTT	1	
SPARTAN@SOAR	4	
TRECS@GEMINI	4	mid-infrared
VIRCAM@VISTA	16	
VISIR@VLT	1	mid-infrared
WIRCam@CFHT	4	